STEM CELLS®
Original Article

Epithelial–Mesenchymal Transition in Colonies of Rhesus Monkey Embryonic Stem Cells: A Model for Processes Involved in Gastrulation

RÜDIGER BEHR,[a] CAROLA HENEWEER,[a] CHRISTOPH VIEBAHN,[b] HANS-WERNER DENKER,[a] MICHAEL THIE[c]

[a]Institut für Anatomie, Lehrstuhl für Anatomie und Entwicklungsbiologie, Universitätsklinikum Essen, Essen, Germany;
[b]Zentrum Anatomie, Abteilung Anatomie/Embryologie, Universität Göttingen, Göttingen, Germany;
[c]Stiftung caesar, Bonn, Germany

Key Words. Embryonic stem cell • Rhesus monkey • Primate • Differentiation • Epithelial–mesenchymal transition Gastrulation • *Brachyury* • *Snail2* • E-cadherin

ABSTRACT

Rhesus monkey embryonic stem (rhES) cells were grown on mouse embryonic fibroblast (MEF) feeder layers for up to 10 days to form multilayered colonies. Within this period, stem cell colonies differentiated transiently into complex structures with a disc-like morphology. These complex colonies were characterized by morphology, immunohistochemistry, and marker mRNA expression to identify processes of epithelialization as well as epithelial–mesenchymal transition (EMT) and pattern formation. Typically, differentiated colonies were comprised of an upper and a lower ES cell layer, the former growing on top of the layer of MEF cells whereas the lower ES cell layer spread out underneath the MEF cells. Interestingly, in the central part of the colonies, a roundish pit developed. Here the feeder layer disappeared, and upper layer cells seemed to ingress and migrate through the pit downward to form the lower layer while undergoing a transition from the epithelial to the mesenchymal phenotype, which was indicated by the loss of the marker proteins E-cadherin and ZO-1 in the lower layer. In support of this, we found a concomitant 10-fold upregulation of the gene *Snail2*, which is a key regulator of the EMT process. Conversion of epiblast to mesoderm was also indicated by the regulated expression of the mesoderm marker *Brachyury*. An EMT is a characteristic process of vertebrate gastrulation. Thus, these rhES cell colonies may be an interesting model for studies on some basic processes involved in early primate embryogenesis and may open new ways to study the regulation of EMT in vitro. STEM CELLS *2005;23:805–816*

INTRODUCTION

Embryonic stem (ES) cell lines have been established from cultures of primate embryos, including rhesus [1], marmoset [2], and cynomolgus monkeys [3] as well as humans [4–6]. Since then, a large number of studies have found that these cells are capable of differentiating into almost all of the specialized cells of the body and, thus, may have the potential to generate replacement cells for a wide range of tissues and organs.

The ability to give rise to differentiated cell types that are derived from all three primary germ layers of the embryo—that is, endoderm, mesoderm and ectoderm—makes ES cells unique. However, our understanding of the developmental potential of ES cells is still fragmentary. Indeed, mouse ES cells have a pattern formation potential that has so far only rarely been studied in detail [7–9]. Although mouse embryoid bodies only partially mimic the early embryonic body plan formation pro-

Correspondence: Hans-Werner Denker, Prof. Dr. Dr., Institut für Anatomie, Lehrstuhl für Anatomie und Entwicklungsbiologie, Universitätsklinikum Essen, Hufelandstr. 55, D-45122 Essen, Germany. Telephone: 49-201-7234380; Fax: 49-201-7235916; e-mail denker@uni-essen.de Received September 9, 2004; accepted for publication February 23, 2005. 1066-5099/2005/$12.00/0 doi: 10.1634/stemcells.2004-0234

cess, particularly striking patterning processes were reported to occur in marmoset monkey ES cell colonies. When grown at high densities, these ES cells have been reported to form embryoid bodies, which, interestingly, have been described to show a close resemblance to early postimplantation embryos, including the formation of a yolk sac, amnion, and embryonic disc with an early primitive streak [2]. Although the identity of the component cells of these structures has not been demonstrated conclusively, the observation has led to the assumption that nonhuman primate stem cells might be good model system for early primate development [10].

ES cells derived from the common marmoset [2] are characterized by a very long replication time and, in addition, a pronounced tendency to differentiate and stop dividing. This makes it difficult to keep them in cell culture for many passages (Thomson, personal communication and unpublished observations) and makes it impossible to obtain sufficient amounts of cells for extensive analyses. Marmoset ES cells are for this reason not commercially available anymore. Therefore, we chose to use the only available rhesus monkey embryonic stem (rhES) cell line, R366.4 [1, 10], to further analyze the differentiation and pattern formation potential of primate ES cells in vitro. Here, we show that under the conditions chosen, these rhES cells can differentiate in vitro into complex structures in which a process can regularly be observed that, according to morphological and molecular characteristics, seems to mimic the epithelial–mesenchymal transition (EMT) as taking place during gastrulation.

Materials and Methods

Culture of rhES Cells

The rhES cell line R366.4 [1, 10] was obtained at passage 14 from the WiCell Research Institute (Madison, WI, http://www.wicell.org). The procedures for propagation of these cells were as follows: rhES cells were grown on mitotically arrested mouse embryonic fibroblasts (MEFs) in a humidified incubator at 37°C in 5% carbon dioxide. The growth medium consisted of Dulbecco's modified Eagle's medium (with L-glutamine, glucose, and pyruvate; Gibco-Life Technology, Karlsruhe, Germany, http://www.invitrogen.com), supplemented with 20% knockout serum replacement (Gibco), 0.1 mM β-mercaptoethanol (Serva, Heidelberg, Germany, http://www.serva.de), 1% nonessential amino acids (Gibco), and 1 mM glutamine (Gibco). The medium was changed daily. Cell colonies composed of closely packed cells were split every 3–4 days by incubation in collagenase IV (0.1 mg/ml, 37°C for 10–20 minutes; Gibco) and pipetting before transfer onto freshly prepared feeder cells.

NMRI mouse embryos at day 13 postcoitum were used as a source of primary cultures of mouse fibroblasts. Cells were mitotically inactivated by mitomycin C treatment (0.06 mg/ml; 37°C for 2 hours; Serva) when they had formed confluent layers. Fibroblasts were directly plated at a final density of 4 to 5×10^5 cells per ml onto tissue culture dishes (24-well plates) pretreated with a solution of 0.1% gelatin. Feeder cell layer density seems to be critical for the reproducible development of the pit-like structures as described in detail in this communication. The optimal feeder cell number was found to be as given above. In contrast to Schulz et al. [11], the time for which feeder cells were cultured did not seem to be critical for pit formation.

The cell line R366.4 was at passage 44 when used for experiments. For differentiation cultures, stem cell colonies were dispersed to small clumps of 5 to 10 cells, washed two times in growth medium, and allowed to grow on mouse fibroblast feeder cells over a period of 4–5 days (immunohistochemistry and in situ hybridization) and 2–10 days (polymerase chain reaction [PCR]), respectively. These culture conditions were chosen to interfere as little as possible with the spontaneous differentiation and pattern formation potential of the ES cells, leaving basically two types of inductive microenvironments: cell-to-cell contacts to adjacent cells within the same colony and cell-to-matrix contacts, i.e., with the networks of macromolecules in the extracellular matrix produced by the underlying mouse feeder layer. Differentiation of colonies was monitored daily by routine phase microscopy until areas containing groove/pit-like structures were identified (usually at day 4). At this time point, colonies were used for analysis.

RNA Isolation and Reverse Transcription–PCR

Total RNA was extracted using the peqGold-TriFast from Peqlab (Peqlab Biotechnologie, Erlangen, Germany, http://www.peqlab.de). Samples were homogenized and incubated for 5 minutes at room temperature (RT). Then 0.2 ml chloroform was added per 1 ml peqGold-TriFast reagent, and the tube was vigorously shaken followed by another 10-minute incubation step. The samples were centrifuged for 5 minutes at 10,000*g*, and the aqueous phase containing the RNA was transferred to another tube. RNA was precipitated over night (O/N) at –20°C after the addition of 0.5 volumes of isopropanol followed by centrifugation at 10,000*g* for 30 minutes at 4°C. The pellet was washed with 70% ethanol (EtOH) in diethylpyrocarbonate (DEPC)–treated water and then dissolved in Tris/EDTA-buffer (TE) (pH 7.5).

One microgram of DNase-treated total RNA was reverse transcribed into cDNA using oligo-dT and random hexamer primers and the Omniscript reverse transcription (Qiagen, Hilden, Germany, http://www.qiagen.com). All primers were purchased from MWG Biotech (Ebersberg, Germany, http://www.mwg-biotech.com). Bio-Therm polymerase (GeneCraft, Münster, Germany, http://www.genecraft.de) was used for PCR. One microliter of cDNA was added to 3 µl 10 × PCR buffer II (including 1.5 mmol/l^{-1} $MgCl_2$), 0.5 µl dNTPs (5 mmol/l^{-1} each), 1 µl of each primer (10 µmol/l^{-1}), 0.5 µl polymerase (2.5 U), and H_2O to a final volume of 30 µl. Standard PCR conditions were 1 × 94°C for 4 minutes, 35 × 94°C for 25 seconds, 60°C for 25 seconds, 72°C for 45 sec-

onds, and 1 × 72°C for 5 minutes. PCR products were separated on 1.5% agarose gels and visualized by ethidium bromide staining. PCR products were ligated into the pCRII vector (Invitrogen, Karlsruhe, Germany, http://www.invitrogen.com) according to the manufacturer's instructions and sequenced (MWG Biotech) to confirm the identity of the amplified fragment.

Quantification of mRNA by Reverse Transcription–PCR

Basically, the procedure was the same as described above. For each mRNA/cDNA, the exponential phase of the PCR was determined by testing different numbers of PCR cycles and subsequent measurement of the signal intensities of the PCR bands. Signal intensity was determined using the Scion imager program (Scion Corporation, Frederick, MD; available at http://www.scioncorp.com/). The concentrations of the cDNA samples from the five time points were equalized by measuring the β-actin PCR signal intensity and subsequent appropriate dilution of samples showing stronger signals. Finally, all tested marker genes were normalized to the β-actin signals obtained after 22 PCR cycles. Primer sequences are available on request.

Digoxigenin-Labeled cRNA Probes for In Situ Hybridization

pCRII vectors containing the respective PCR fragments were linearized with BamH I or XhoI. In vitro transcription of the linearized plasmids into digoxigenin (DIG)–labeled cRNA was performed using the 10 × RNA-DIG Labeling-Mix (Roche Biochemicals, Mannheim, Germany, http://www.roche-applied-science.com) and RNA-polymerases T7 and SP6, respectively. Quality and efficiency of the cRNA synthesis were tested by RNA gel electrophoresis.

In Situ Hybridization

Samples were fixed for 30 minutes at room temperature in 4% (para)formaldehyde in 1 × PBT (1 × phosphate-buffered saline [PBS] plus 0.1% Tween 20). After fixation, the cells were washed in 1 × PBT at RT. Next the cells were acetylized for 10 minutes in acetic acid anhydride followed by another 2 washes in 1 × PBT. Incubation in prehybridization buffer (50% deionized formamide, 5% dextrane sulfate, 1 × Dehnhardt's solution, 4 × standard saline citrate [SSC], pH 4.5, 0.25 mg/ml yeast t-RNA) was carried out for 2 hours at 53°C. For hybridization, the probe was denatured for 5 minutes at 65°C in 10 µl of hybridization buffer (prehybridization buffer plus 0.5 mg/ml denatured salmon sperm DNA). Then the probe was added to the colonies in the wells. Hybridization was carried out O/N at 53°C. Then the colonies were washed two times for 15 minutes in 5 × SSC at RT, one time for 1 hour in 0.2 × SSC at 53°C, and finally one time for 15 minutes in 1 × PBT at RT. Unspecifically bound cRNA was removed by RNase (20 µg/ml) digestion for 15 minutes at 37°C. The DIG-labeled probe was visualized using an alkaline phosphatase (AP)–conjugated anti-DIG antibody (DAKO, Hamburg, Germany, http://www.dakocytomation.de). Endogenous AP was inhibited with levamisole (4.8 µg/ml), which was added to all solutions. Unspecific binding of the antibody was inhibited by incubation with 2% sheep serum in buffer (100 mM maleic acid, 150 mM NaCl, pH 7.5) for 30 minutes before antibody incubation (1:500 dilution in maleic acid buffer plus 1% sheep serum) at 4°C O/N. The AP-staining reaction was done with 5-bromo-4-chloro-3-indolyl phosphate, toluidine salt (Roche Diagnostics, Mannheim, Germany, http://www.roche-diagnostics.com) as substrate and Nitro blue tetrazolium chloride in 100 mM Tris/HCl buffer, pH 9.5, 100 mM NaCl, 50 mM $MgCl_2$. The staining reaction was stopped after 2–4 hours by replacing the staining solution with 1 × TE for 5 minutes. Finally the cells were washed with Aqua destillata (distilled water), air dried, and mounted with Mowiol (Kuraray Specialities Europe, Frankfurt/Main, Germany, http://www.kuraray-kse.com).

Alkaline Phosphatase Staining

Alkaline phosphatase activity was detected histochemically after fixation of cells with 100% ethanol using the alkaline phosphatase staining kit (86R) obtained from Sigma Diagnostics (St. Louis, http://www.sigmaaldrich.com). The staining procedure was carried out as recommended by the manufacturer. Micrographs of samples were taken using an Axiovert 100M microscope (Carl Zeiss, Jena, Germany, http://www.zeiss.com).

Immunohistochemistry and Actin Staining

As an epithelial cell marker and an indicator of apico-basal polarity, the tight junction-associated protein ZO-1 was used. In addition, E-cadherin (E-cad) was used as one of the prototypic markers of epithelial cells. Connexins (Cx43 and Cx32) were used as markers for epiblast versus hypoblast [12]. Rabbit polyclonal antibodies to human ZO-1 (61-7300) were obtained from Zymed WAK Chemie (Bad Homburg, Germany, http://www.zymed.com) and used in 1:200 dilution in PBS supplemented with 0.5% bovine serum albumin (BSA). A mouse monoclonal antibody (C 20820) against a fragment of human E-cad (amino acids 735–883) was obtained from Transduction Laboratories (Lexington, KY, http://www.bdbiosciences.com/pharmingen) and used in 1:100 dilution in PBS supplemented with 0.5% BSA. Rabbit polyclonal antibodies to human Cx43 (71-0700) and Cx32 (71-0600) were obtained from Zymed WAK Chemie and used in 1:50 (Cx43) and 1:200 (Cx32) dilution in PBS-BSA. The secondary antibodies, Alexa Fluor 633–conjugated goat anti-rabbit immunoglobulin G (IgG) (A-21071) and Alexa Flur 488–conjugated goat anti-mouse IgG (A-11017), were obtained from Molecular Probes (MoBiTec, Göttingen, Germany, http://www.mobitec.de) and used in 1:200 dilution in PBS-BSA. Tetramethylrhodamine isothiocyante (TRITC)–conjugated phalloidin

was obtained from Sigma-Aldrich (Taufkirchen, Germany) and used at a concentration of 25 µg/ml in PBS to stain F-actin. Rhesus monkey liver sections were used as positive control for Cx32 and heart sections for Cx43 staining.

Immunostaining was performed as follows: samples were fixed in a 1:1 mixture of ethanol:acetone for 10 minutes at RT. Nonspecific binding of the antibodies was blocked by incubation with PBS-BSA for 15 minutes, followed by incubation with the primary antibody (see above) for 90 minutes at RT. The primary antibody was omitted in control stainings. Thereafter, cells were rinsed in PBS-BSA, incubated with the corresponding fluorescence-conjugated secondary antibody (see above) for 60 minutes at RT, and mounted in glycerol (90%)/PBS (9%)/p-phenylenediamine (1%). F-actin staining was performed as follows: samples were fixed with 3.5% (para)formaldehyde for 15 minutes at RT, permeabilized by incubation with 0.05% Triton X-100 for 2 minutes, and incubated for 15 minutes with TRITC-phalloidin before mounting in PBS/glycerol/phenylenediamine. To combine immunofluorescence and F-actin staining, samples were fixed in formaldehyde and permeabilized in Triton X-100 according to the actin-staining protocol. Then the primary antibody and the TRITC-phalloidin were applied simultaneously, while both were omitted in controls. Thereafter, the immunostaining reaction was performed as described above.

Confocal Laser-Scanning Microscopy

Confocal microscopy was performed using a Zeiss Axiovert 100M microscope attached to a confocal laser-scanning unit (model LSM 510; Carl Zeiss) as described previously [13, 14]. One argon laser with output at 488 nm as well as two helium-neon lasers with output at 543 and 633 nm, respectively, were used as excitation sources. TRITC fluorescence was imaged with a 560- to 565-nm bandpass filter, Alexa Fluor 633 fluorescence with a 650-nm longpass filter, and Alexa Fluor 488 fluorescence with a 505- to 530-nm bandpass filter. Optical tomography was performed at 0.8-µm intervals using a 20-fold objective and a pinhole size corresponding to a value of 1.0 of the airy disk. Each slice was scanned eight times followed by averaging of the obtained images to improve the signal-to-noise ratio.

Electron and Light Microscopy

Cells were grown on thermanox coverslips (Nunc, Naperville, IL, http://www.nuncbrand.com) as described above. For subsequent electron microscopy, samples were rinsed twice in PBS and fixed in 2.5% glutaraldehyde in 0.1 M cacodylate buffer, postfixed with 1% OsO_4 in cacodylate buffer, dehydrated with ethanol and propylene oxide, and embedded in epoxy resin. The embedded cells were separated from the thermanox coverslips by snap freezing in liquid nitrogen. Ultra-thin sections (90 nm) were mounted on 200 mesh copper grids, double-stained with uranyl acetate and lead citrate, and examined with a Zeiss EM 510 at 80 kV. For light microscopy, thin sections (1 µm) were mounted on glass coverslips and stained in 1% toluidine blue. Samples that were processed for in situ hybridization were sectioned at 8 µm and examined without toluidine staining.

Image Processing

Image enhancement was performed with Image Pro Plus software (version 4.5; Media Cybernetics, Crofton, MD, http://www.mediacy.com) equipped with a Gaussian filter module [15] and a homomorphic filter plug in. Adobe Photoshop software (version 5.0; Adobe Systems Inc., San Jose, CA, http://www.abode.com) was used for arrangement of RGB-color images.

Results

General Morphology

Confluent monolayers of MEFs were cultured on gelatin-coated tissue culture dishes and used as feeder cells to grow the rhES cell line R366.4 for up to 10 days. During the day after seeding, ES cells attached to the free surface of the mouse feeder and formed small colonies as previously described [1, 10]. Growth and development of ES cells were monitored daily.

Over the first days, stem cell colonies increased in size and cell number and became more compact. After 3–4 days of continuous growth, colonies differentiated into more complex structures, i.e., they became roundish and flattened but multilayered. Using phase-contrast microscopy, after 3–4 days of culture, pit-like depressions became visible in the centers of almost all colonies.

Typically, the disc-like colony was multilayered, i.e., it was composed of an upper and a lower layer, and between both ES cell layers the layer of MEF cells was positioned (Fig. 1). At the periphery of the colony, the upper and the lower ES cell layers were completely separated by the MEF layer—that is, one sheet of cells was growing on top of the feeders, thereby covering the latter, and the other was growing below the feeder cell layer, thereby fixing the colony to the culture dish (Figs. 1A–1F, 1K). However, at the described pit in the center of the colony, the upper and the lower ES cell layers were in continuity—that is, not separated by the feeder cells (Figs. 1D, 1E, 1J). The diameters of the pits were varying between the colonies. Detailed histological examination of the centers clearly revealed that the mouse feeder cells were completely absent from these areas of the colonies (Figs. 1H–1J). The feeder layer between the ES cell layers thickened toward the periphery to reach its normal dimension as outside of the colony (Figs. 1J, 1K). Within the developing pit, the cells from the upper layer appeared to move while still in contact with their neighbors, through the feeder cell layer into the space between the feeder cells and the culture dish, thereby forming the lower layer (Figs. 1H–1K). The pit diameter increased during continuing growth of the colony. In widened flat-bottomed pits, epithelial cells obviously derived from the upper layer formed the bottom of the pit

(Figs. 1D, 1E, 1J). In such enlarged pits, feeder cells had completely disappeared. Mixing of cells from the upper layer or from the lower layer of ES cells with those from the mouse feeder layer was never observed.

This regular morphology of the colony with a central pit was observable for only a relatively short period of approximately 2 days until colonies grew together and proliferated or migrated in a more uncoordinated fashion.

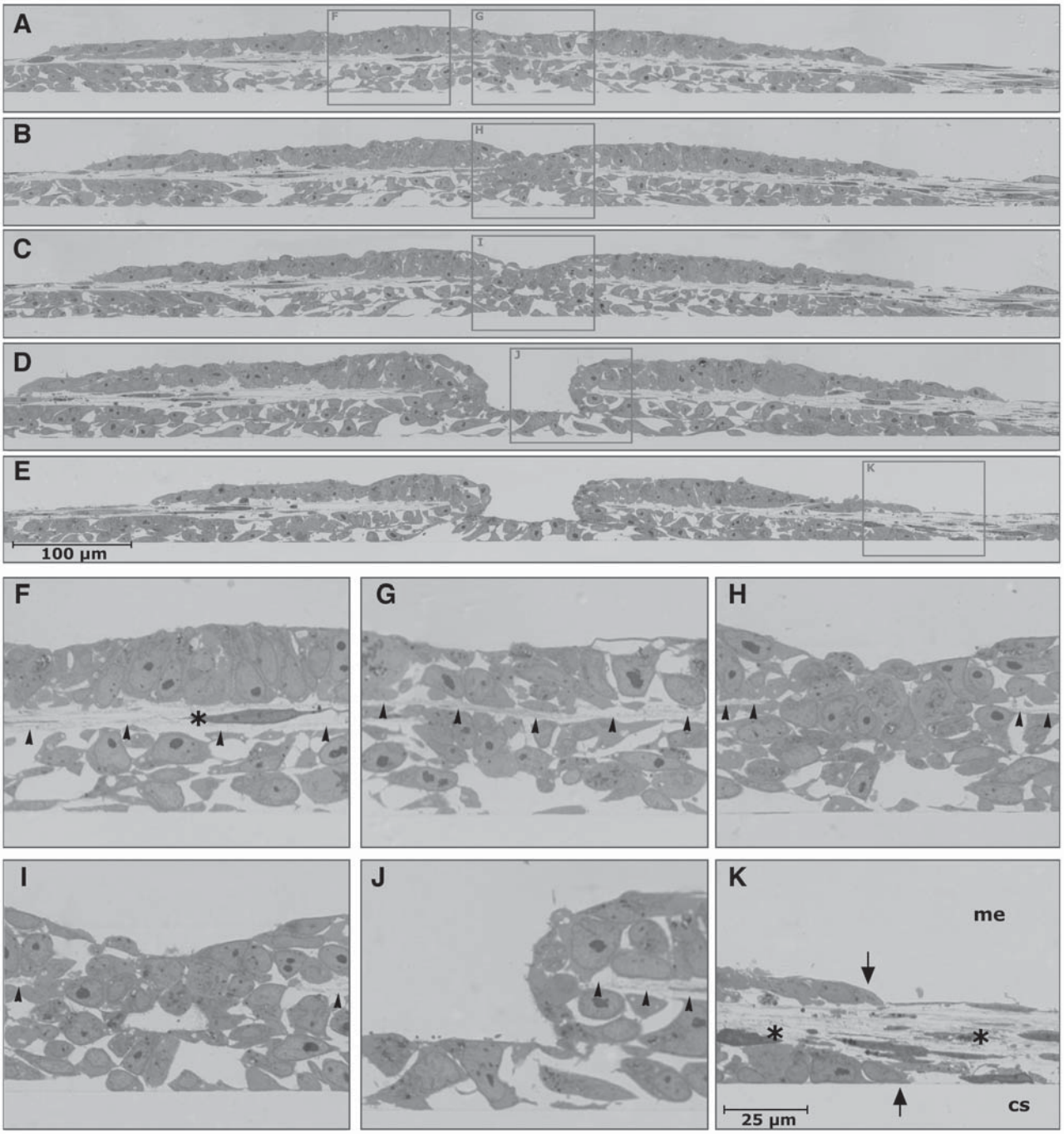

Figure 1. A typical differentiated colony of rhesus monkey embryonic stem cells after 5 days of culture in a series of cross-sections starting from the **(A)** periphery of the colony and continuing toward the **(E)** center. When viewed from the side, the differentiated colony is comprised of an upper and a lower layer and, between the two, the **(A)** preexisting layer of mouse feeder cells. **(E):** Note the lack of the feeder layer in the central region of the colony where the pit-like structure emerges. **(F–K):** Enlargements of the boxed areas in **A–E**. They show details of the arrangement of stem cells and feeder cells. Arrowheads indicate mouse feeder layer; asterisks, mouse embryonic fibroblasts embedded within the matrix of the feeder layer; arrows, stem cells from the upper and the lower layer, respectively, located at the periphery of the colony. Abbreviations: cs, coverslip; me, medium.

Ultrastructural Features

Cells of the upper layer of the colonies exhibited epithelial-like characteristics with specialized cell-cell junctions anchored by prominent bundles of filaments in their apical cell pole (Figs. 2A, 2C). These cells were clearly polarized, with their tight junctions being located in the subapical region while the remainder of the lateral plasma membrane showed only few punctual adherens junctions, and here the intercellular space was wide. The apical surface of cells showed microvilli-like structures as well as plump cytoplasmic protrusions. The cells had a low nucleus-to-cytoplasm ratio and prominent nucleoli. Most of these cells showed a polarized organization of the cytoplasm, organelles being concentrated in the apical part of the cell and the nucleus close to the basal pole. Via their basal pole, almost all cells were in direct contact with a supporting matrix provided by the feeder cell layer (Fig. 2A). Electron microscopically, this matrix showed collagen fibrils, but the composition of this matrix was not analyzed in further detail. No electron-dense structure resembling a basement membrane was found.

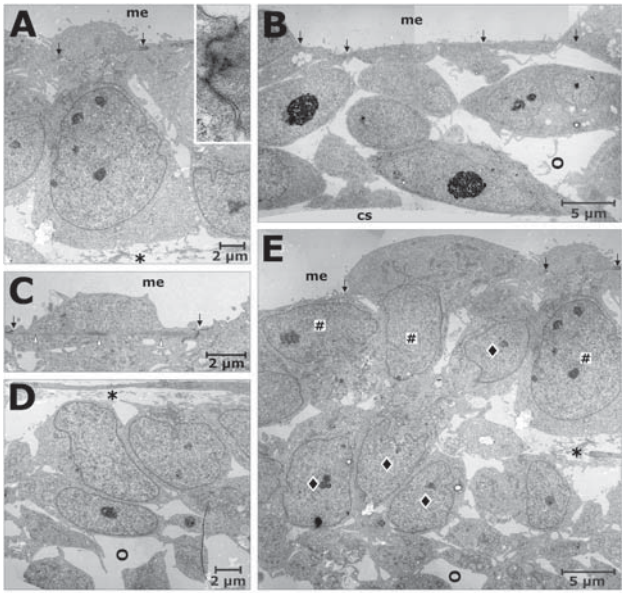

Figure 2. Electron micrographs of a differentiated rhesus monkey embryonic stem cell colony. Cells within the **(A, C)** upper layer are epithelioid, whereas **(D)** lower layer cells have a mesenchyme-like phenotype. The epithelioid cells are apico-basally polarized, showing specialized cell–cell junctions in their apical pole **(C,** inset in **A)**. The depressed region of the central part of the colony (pit) is several cells thick, and **(B)** only the uppermost cells are connected by tight junctions as is typical for an epithelium. **(E):** As observed in the lateral region of the central pit, cells from the upper layer seem to undergo a modulation of their phenotype, to ingress, and to migrate downward to form the lower layer. Asterisk indicates mouse feeder layer; arrowheads, prominent bundles of filaments in epitheloid cells; arrows, specialized cell–cell junctions between epitheloid cells; O, intercellular space within the colony; #, epithelioid cell; ◊, migrating mesenchyme-like cell ingressing from the upper layer. Abbreviation: me, medium.

While the epithelial cells of the upper layer of the colony were usually attached to the feeder layer, cells within the pit lacked this support layer. Cells in the pit were usually multilayered, but typically only the upper cells facing the medium were tightly connected with each other via tight junctions, thus clearly exhibiting an epithelial phenotype. The cells of the lower layer were attached to each other via primitive punctate membrane contacts, thereby forming a loose network. These cells developed long extrusions that reached into the space surrounding the cells (Fig. 2B). The lowest cells constituting the bottom of the pit had a broad contact area with the matrix of the culture dish.

Outside the pit, the ES cells of the lower layer of the colony had a mesenchymal phenotype (Figs. 2D, 2E). They exhibited a high nucleus-to-cytoplasm ratio, were irregular in shape (polygonal), and lacked regular cell-cell contacts and apico-basal polarity. In the vicinity of the pit, cells looked scattered, suggesting that cells had acquired here a migratory phenotype (Fig. 2E). Probably these cells had moved down from the upper layer and continued now to migrate into the space between the feeder cell layer and the culture dish, thereby forming the pit-like structure of the colony.

Distribution of ZO-1, E-cad, and Cx43

As mentioned above, epithelial-like cells were formed in the upper layer of differentiated stem cell colonies. Here, we further analyzed the nature of specialized junctions between these cells. Of particular interest are occluding junctions (tight junctions) as they are typical of epithelial cells. Occluding junctions seal cells together in an epithelial sheet. Moreover, we characterized E-cad–mediated cell–cell adhesion, which is strictly regulated during mesoderm formation [16], and also the communicating junctions, which mediate signals from one cell to its interacting partner. As marker molecules for these different types of junctions, we have chosen the tight junction protein ZO-1 (Figs. 3A–3F), the epithelium-specific cell–cell adhesion protein E-cad (Figs. 3G–3L) [17], and the gap junction proteins Cx43 and Cx32, the latter being markers for epiblast and hypoblast, respectively [12] (Figs. 4A–4F).

ZO-1 immunohistochemistry revealed that the upper layer (Figs. 3A, 3D) but not the lower layer (Figs. 3C, 3F) was comprised of ZO-1–positive cells. The tight junction protein ZO-1 was found at the subapical part of the lateral border of adjacent cells in the top layer cells, as were tight junctions in transmission electron microscopy (see Fig. 2). In contrast, ZO-1 was only very weakly detectable in cells of the lower layer (Figs. 3C, 3F). E-cad was found to be strongly expressed in adhesion belts of the epithelial cells in the top layer (Figs. 3G, 3J, 3M) and in those cells lining the pit in the center of the colonies (Fig. 3H, 3K). In contrast, E-cad largely disappeared in the cells of the lower layer (Figs. 3I, 3L, 3M). This change of marker expression correlates well with the morphological changes observed in these cells (see Figs. 1, 2). Thus, the upper layer cells that are covering the surface of the

colony can be characterized as an epithelium, including those cells that were lining the pit in the center of the colonies (Figs. 3B, 3E, 3H, 3K), creating a seal that isolates the interior of the colony from the external medium.

Upper layer cells also were coupled via gap junctions, as suggested by their expression of connexin Cx43 (Figs. 4A–4F). Epithelial cells of the outermost layer in the periphery (Figs. 4A, 4D) as well as in the center of the pits (Figs. 4B, 4E) showed a clearly positive immunohistochemical signal for Cx43. Confocal microscopy revealed a web-like pattern, suggesting that gap junction protein Cx43 was localized within lateral membrane domains of adjacent cells. With respect to the mesenchyme-like cells of the lower layer, Cx43 fluorescence was significantly weaker in many places (Figs. 4C, 4F), and instead of web-like patterns, weak spotty signals were found irregularly distributed within the cells. In contrast to Cx43, Cx32 was observed neither in cells of the upper layer nor in those of the lower layer, whereas monkey liver exhibited a strong and specific signal (positive control; data not shown).

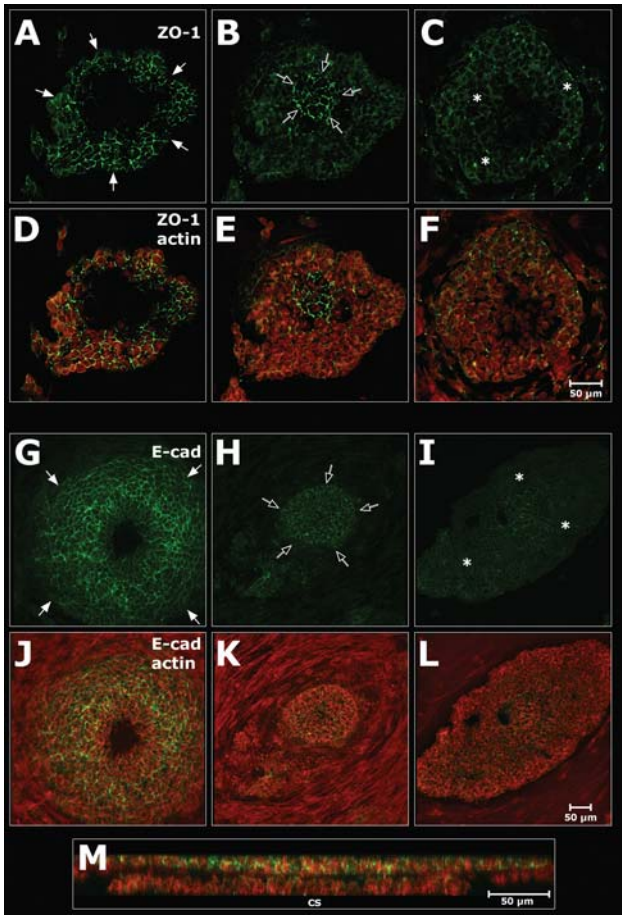

Figure 3. Typical localization of **(A–F)** the tight junction protein ZO-1 and the **(G–M)** cell–cell adhesion protein E-cad together with **(D–F, J–M)** F-actin in differentiated colonies of rhesus monkey embryonic stem cells as shown by confocal laser-scanning microscopy. Optical sections are from **(A, D, G, J)** the upper layer of the colony, grazing the **(B, E; H, K)** pit in the center of the colony and the **(C, F; I, L)** lower layer. Note the web-like staining pattern of both ZO-1 and E-cad in the upper layer (white arrows) and the top cells in the pit (black arrows), respectively. In contrast, cells of the lower layer showed only weak and rather irregular staining of ZO-1 and E-cad (asterisks). **M**, An E-cad stained colony in an xz-section. Green staining representing E-cad is much stronger in the upper layer compared with the lower layer of the colony. Abbreviations: CS, coverslip; E-cad, E-cadherin.

Expression of ES Cell–Specific Markers

Established ES cell markers include alkaline phosphatase, the POU domain gene product *Oct-4*, and telomerase reverse transcriptase [6, 18], all known to be involved in or associated with pluripotency of embryonic stem cells; i.e., their expression was reported to decrease upon stem cell differentiation. After forming morphologically differentiated colonies, rhES cells still expressed all markers tested, as revealed by histochemistry (alkaline phosphatase, Fig. 5A), in situ hybridization (*Oct-4*, Fig. 5B), and reverse transcription–PCR (*Oct-4* and Tert, Figs. 5C, 5D). Interestingly, the mRNA levels of Tert strongly decreased between days 2 and 4 of the culture and remained low thereafter. In contrast, the expression of *Oct-4* continuously increased during the differentiation of the colonies. At day 10, the mRNA abundance of *Oct-4* was approximately 2.3-fold higher than in day-2 colonies. This shows that the expression of *Oct-4* and Tert, both reported to be markers for pluripotent stem cells, diverges in differentiating rhES cell colonies. Interestingly, in situ hybridization revealed that almost all cells within a colony contained *Oct-4* mRNA, although at the stage of colony development shown in Figure 5B, a large subpopulation of cells in the colony had already differentiated to epithelial cells (compare with Figs. 3, 4).

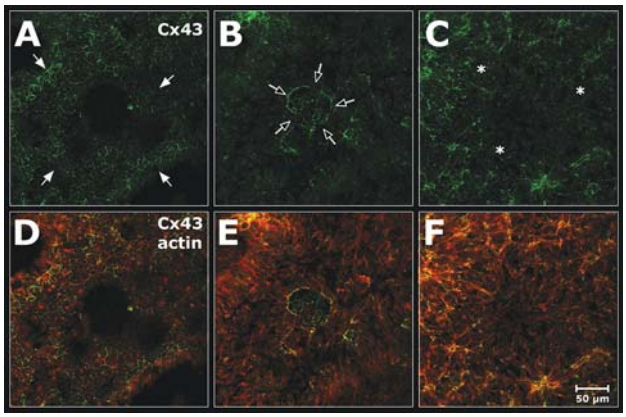

Figure 4. (A–F): Typical localization of the gap junction protein connexin Cx43 together with **(D–F)** F-actin in differentiated colonies of rhesus monkey embryonic stem cells as shown by confocal laser-scanning microscopy. **(A, D):** Optical sections are from the upper layer of the colony, grazing the **(B, E)** pit in the center of the colony and the **(C, F)** lower layer. Note the web-like staining pattern of Cx43 in the upper layer (white arrows) and the top cells in the pit (black arrows). In contrast, cells of the lower layer showed only weak and rather irregular staining of Cx43 (asterisks).

Expression of Developmental Marker Genes

Since morphological observations made in marmoset monkey ES cell colonies [2] had suggested that primitive streak equivalents can form there, we wished to obtain information on EMT- and gastrulation-related gene expression in differentiating rhES cell colonies. This was done by in situ hybridization (Fig. 6) and quantitative reverse transcription–PCR (Fig. 7) on cDNA isolated from colonies of different developmental stages. The transcription factor genes *Brachyury, goosecoid, Snail2,* and *MesP2* (primate *MesP2* is more closely related to mouse *MesP1* than primate *MesP1* and was therefore investigated in this study) were investigated as markers for gastrulation. *Brachyury* is a reliable marker for mesoderm progenitor cells in normal embryos. Its expression is induced in epiblast cells of the rabbit several hours before the first visible signs of primitive streak formation and EMT [19]. *Brachyury* was strongly expressed in our experimental system in day-2 colonies as revealed by reverse transcription–PCR (Fig. 7). During further differentiation of the colonies, the expression level of *Brachyury* continuously and dramatically decreased. At day 10, there was almost no *Brachyury* mRNA detectable. In the rhES cell colonies, *goosecoid* mRNA abundance increased between days 2 and 4. Thereafter, *goosecoid* signal intensity clearly decreased and dropped to low levels at day 10 (Fig. 7). In contrast to *Brachyury* and *goosecoid*, *Snail2* (or *Slug*), a gene specifically expressed in the embryo in early mesodermal cells emigrating from the primitive streak and undergoing an EMT [20], was more than 10-fold upregulated between days 2 and 6. *MesP1* expression in the mouse embryo was first observed at the onset of gastrulation in the nascent mesodermal cells that first ingressed at the end of the primitive streak [21]. The abundance of *MesP2* mRNA increased approximately twofold in the rhES cell colonies between days 2 and 6. E-cad mRNA signal increased between days 2 and 4, remained high until day 8, and slightly declined thereafter. This may reflect the formation of epithelial sheets followed by a relative decrease of epithelial cells during formation of lower-layer mesenchymal cells at the later stages.

In situ hybridization on whole differentiated colonies from day 4 with probes specific to *Brachyury* and *goosecoid* revealed that both marker genes were detectable in the cytoplasm of both cell layers of the colonies (Fig. 6C). However, a pattern or confinement of the signal to single cells or clusters of cells within the colonies could not be observed. Specificity of the hybridization signal was shown by the fact that neither the nuclei of the ES

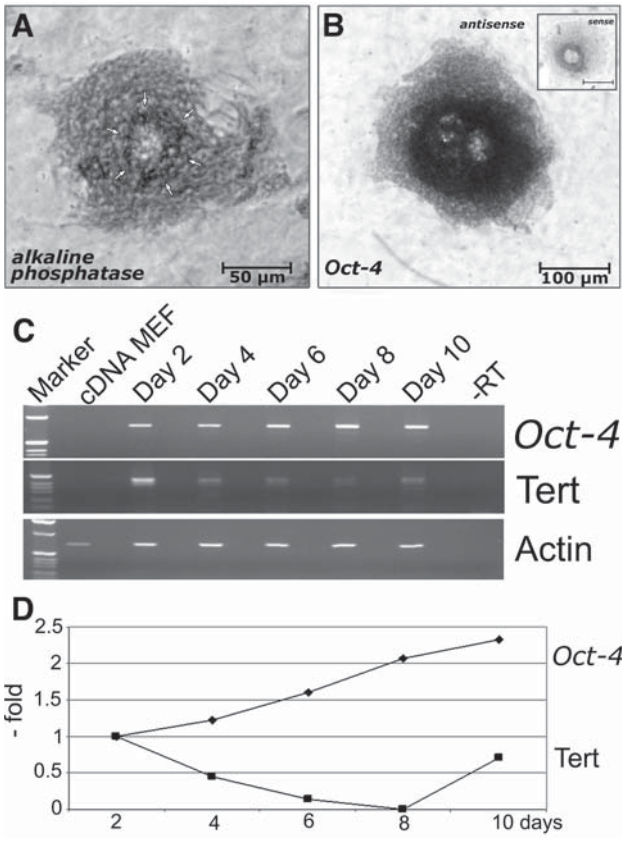

Figure 5. Full-face view of differentiated colonies of rhesus monkey embryonic stem (rhES) cells after **(A)** alkaline phosphatase staining and **(B)** whole-mount in situ hybridization with *Oct-4*, respectively. Alkaline phosphatase and *Oct-4* are detectable in almost all cells of the colony. The upper layer of the colony is marked (arrows in **A**). **(C, D):** Quantification of undifferentiated stem cell marker mRNA expression in rhES cells after 2, 4, 6, 8, and 10 days of culture. **(C):** The mRNA for the transcription factor *Oct-4* was clearly upregulated, whereas the telomerase reverse transcriptase (Tert) mRNA was downregulated during the experimental period. **(D):** Quantification of the signals shown in **(C)**. The value determined for day 2 was set as 1. All other values given are relative to this time point. Abbreviation: MEF, mouse embryonic fibroblast.

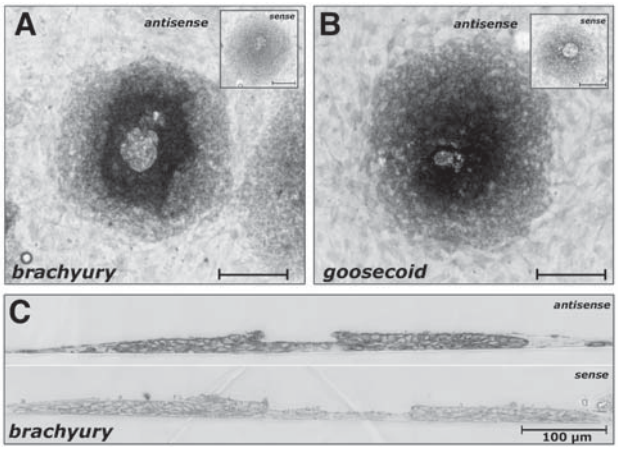

Figure 6. (A): *Brachyury* and **(B)** *goosecoid* expression in differentiated colonies of rhesus monkey embryonic stem cells as revealed by in situ hybridization (full-face view). **(C):** Cellular distribution of *Brachyury* expression as seen in cross sections. Note that *Brachyury* transcripts are not restricted to a specific layer or cell population of the colony but are found in all cells irrespective of their position. Mouse embryonic feeder cells show no staining.

cells nor the mouse feeder cells showed any significant staining with the antisense probe (Fig. 6C). Moreover, the sense controls showed almost no staining.

Discussion

ES cells are widely being investigated with a focus on their pluripotent properties, i.e., their ability to differentiate into a broad array of cell types potentially useful as cell material for purposes of regenerative medicine [22]. On the other hand, ES cells also have, in parallel to this cell-differentiation potential, a remarkable ability to initiate pattern formation as evidenced by experiments on teratoma formation [23–26]. Although it has indeed been suggested before that ES cells may be a useful model system for investigations on embryonic development [2, 9, 10], pattern formation in the strict sense has rarely been the focus of ES cell research so far, in striking contrast to cell-differentiation research.

We used the rhES cell line R366.4 [1] to investigate the potential of primate ES cells to recapitulate certain basic processes of the early phases of primate embryogenesis, specifically processes of EMT involved in gastrulation and the formation of the three germ layers in vitro. This study was prompted by the report of Thomson and colleagues that marmoset ES cells can differentiate into embryoid bodies closely resembling the early trilaminar postimplantation embryo, including the formation of an embryonic disc–like structure with an early primitive streak, an amnion, and a yolk sac [2]. However, this was not reported to occur in rhES cell colonies [1]. Because marmoset ES cells are not available anymore, we investigated colonies formed spontaneously in culture by rhES cells, focusing on morphology as well as on expression of proteins and genes of interest. Here, we provide evidence that rhES cells differentiate in vitro into complex structures with some degree of morphological order, in which a coordinated EMT process is locally initiated that may indeed be somewhat reminiscent of processes occurring in normal embryogenesis during gastrulation.

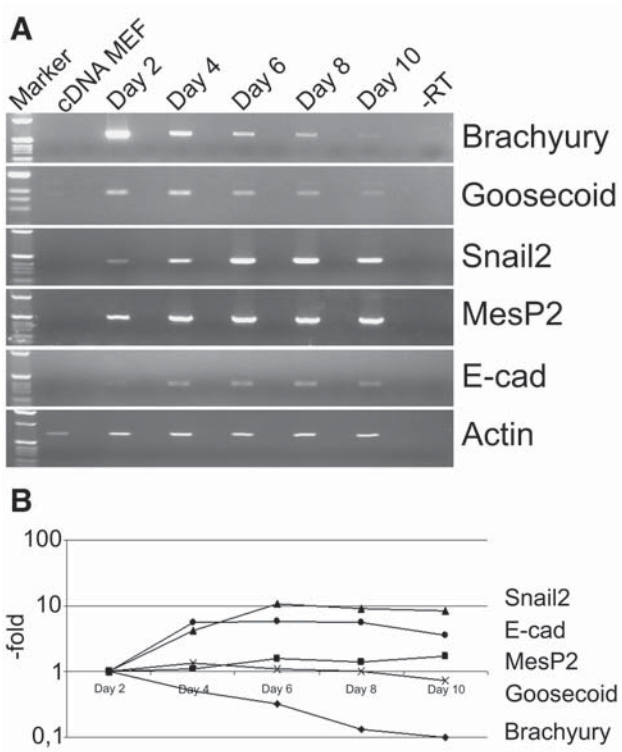

Figure 7. Quantification of marker mRNA expression in rhesus monkey embryonic stem cells after 2, 4, 6, 8, and 10 days of culture. **(A):** The mRNAs for the transcription factors *Brachyury* and *goosecoid* are clearly downregulated during the experimental period. In contrast, the transcription factors *Snail2* and *MesP2* are upregulated during the first days of culture, whereas E-cad signal intensity increases until day 4 and slightly decreases at day 10. **(B):** Quantification of the signals shown in **(A)**. The value determined for day 2 was set as 1. All other values given are relative to this time point. All values were normalized to β-actin. Abbreviations: E-cad, E-cadherin; MEF, mouse embryonic fibroblast.

Before gastrulation, the primate embryo exhibits a bilaminar embryonic disc consisting of a distinct upper layer, called the epiblast, and a lower layer, called the hypoblast. With the onset of gastrulation, the bilaminar embryonic disc is converted into a trilaminar one. Gastrulation starts with the appearance of the primitive streak (primitive pit, primitive node) in the epiblast when epiblast cells begin to immigrate, undergoing the process of EMT and migrating into the potential space between the epiblast and the hypoblast. Replacing the hypoblast, some of these cells also form the (definitive) endoderm; other cells that migrate between the hypoblast (and later endoderm) and the epiblast form the mesoderm. After gastrulation, the remaining cells of the epiblast are called the ectoderm.

Colonies of rhES cells spontaneously differentiating in vitro on MEF cell monolayers in our experiments did not develop to a fully organized and normally structured embryonic disc. Also, there was no formation of an amnion or a yolk sac. However, the colonies did mimic some features of a bilaminar embryonic disc, and we found evidence that rhES cells have the ability to initiate a remarkably ordered process somewhat reminiscent of one of the main features of normal gastrulation, i.e., mesoderm formation through EMT. The structures we found here were composed of an upper and a lower layer. While the upper layer showed morphological and immunohistochemical characteristics of an epithelium, cells in the lower layer lacked these characteristics or at least presented them in a strongly reduced form. The lower layer cells appeared to have undergone a process of EMT while cells were migrating into the lower compartment. A clear difference in comparison with gastrulation in vivo, however, was that the layer of mouse feeder cells remained interposed between the upper epithelium and the lower layer, somewhat acting like a hinge region for the ingression of the lower layer cells. Moreover, the central pit of the colony where signs of EMT could be found became much wider than a normal primitive streak or groove in vivo. Neverthe-

less, the degree of order seen in these colonies with respect to the formation of the pit and the regular occurrence of the pits was an unexpected finding. Furthermore, it seems interesting that the pit was regularly located in the central part of the colony, suggesting that a certain cell density might suffice, perhaps in concert with signaling molecules from the feeder cells, to trigger EMT. Morphology as well as immunohistochemistry suggested that at this specific site, upper-layer epithelial cells undergo changes concerning structure, gene expression, and cell behavior and ingress, i.e., they move downward underneath the original epithelium as well as the underlying feeder cell layer to form a new, lowest cell layer. We identified those cells in the upper layer as epithelial-like cells not only on the basis of their morphological characteristics but also on the typical expression patterns of the tight junction protein ZO-1 and the adhesion junction protein E-cad, which is exclusively expressed in epithelia [17]. Because the junctions seen in transmission electron microscopy (Fig. 2) as well as the ZO-1 spots and the E-cad signal revealed by confocal laser-scanning microscopy (Fig. 3) were localized in the subapical part of the lateral plasma membrane, this epithelium was clearly polarized. In addition, these cells also expressed the gap junction protein Cx43 (Fig. 4), which is an epiblast marker in the embryonic disc of other species (mouse [27, 28], rat [29], and rabbit [12]). In good agreement, Cx43-positive cells did not react to antiCx32, which is known to be exclusively expressed in the hypoblast and yolk sac epithelium of the intact germ disc in the rabbit but not in the epiblast [12]. Interestingly, those cells that seemed to ingress at the pit from the upper layer showed strongly reduced levels of ZO-1 and Cx43 expression. Moreover, E-cad signals largely vanished in the lower layer. The downregulation of these proteins coincided with a change in the morphological characteristics of cells, i.e., the cells lost their epithelial organization and adopted a scattered, mesenchymal phenotype. These data were supported by the increased expression of the transcription factor *Snail2* occurring at the stages when the pits developed. This factor generally functions as a repressor of epithelial phenotypes and was considered as a causative key factor for EMT processes. *Snail2* represses E-cad expression. E-cad, again, plays an important role during the EMT processes [30, 31].

Our morphological as well as our molecular data presented thus far suggest that the rhES cells are indeed undergoing an EMT at the pit. However, it is still of great interest to what extent this EMT is comparable to the EMT that characterizes gastrulation in vivo [20, 31, 32]. In mouse and rabbit, *Brachyury* is first expressed in the posterior epiblast (which still is epithelial) at the site where the primitive streak forms and then in the migratory primitive streak mesoderm [19, 33, 34]. *goosecoid* is also expressed in epithelial cells of the epiblast at the site where the primitive streak is first formed and subsequently in mesodermal cells of the early gastrula [35]. Thus, our findings of *Brachyury* and *gooseecoid* expression in the upper epithelial cell layer as well as in the lower mesenchymal layer of the rhES cell colonies are consistent with the in vivo situation. Our interpretation is that the colonies described here are indeed composed of epiblast-like cells and (migratory) mesoderm cells, forming a structure that has some resemblance of a primitive pit.

Interestingly, all cells of the upper and lower layer of colonies were alkaline phosphatase–positive and *Oct-4*–positive. The expression of these markers is generally considered to decrease upon stem cell differentiation. However, careful evaluation of the literature shows that *Oct-4* is not as strictly restricted to stem cells/inner cell mass (ICM) or totipotent precursor cells, as is often suggested. Yeom et al. [36] showed that *Oct-4* is expressed in the mouse embryo not only up to the blastocyst stage but also in the epiblast up to the gastrulating stage embryo. Moreover, *Oct-4* expression persists in the mouse embryo through day 7.5 in the unsegmented presomitic mesoderm [37]. In contrast to *Oct-4*, Tert expression seems to be much more closely associated with the stem cell character, because its expression clearly decreased with increasing differentiation of the rhES cell colonies (Fig. 5). This is in agreement with data reported by Armstrong et al. [38], who showed that the expression of mouse Tert was substantially reduced upon differentiation of ES cells into more committed lineages.

In conclusion, our data suggest that the rhES cell line R366.4 may represent a source of embryonic progenitor cells that not only may be able to form colonies with an epiblast-like epithelium but also seem to go on spontaneously to form, in turn, mesoderm during a process of EMT that bears some remarkable resemblance to what is going on in a primitive streak in vivo. In our model system, ES cell marker gene expression, on the one hand, and morphological differentiation and marker gene expression for gastrulation, on the other hand, clearly do overlap. This might be, at first glance, surprising. However, the previously described gene expression data from nonprimate species (as cited above) do not necessarily argue against the hypothesis that the succession of marker gene upregulation and downregulation occurring in the rhES cell colonies does perhaps mimic aspects of primate embryo development in vivo. However, for reasons of comparability and certainty, it would be of great interest to analyze the corresponding gene expression patterns in appropriate stages of in vivo–developed rhesus monkey embryos. Because such series of rhesus monkey embryos are not available to us, correlation with the in vivo situation must so far rely on interspecies comparisons (mouse, rabbit, and chicken) and remain partly speculative.

Under the present culture conditions, rhES cell colonies did not reach a degree of structural organization that comes close to what Thomson et al. [2] had described as well-organized germ discs in marmoset ES cell cultures. It is not clear whether this difference reflects differences in the developmental potential between the marmoset and rhesus monkey ES cells or may result from other variations, e.g., the developmental stage at which

the blastocysts/ICM were recovered. It is also conceivable that differences in the procedures of isolating or selecting the cells or the number of passages may influence their in vitro potential [39]. Moreover, failure of proper embryonic disc formation may be due to the lack of key factors or conditions necessary for directing a colony to a normally structured gastrula-like stage. Because we were not able to surely identify hypoblast-like cells (although we could clearly detect *HNF4*α mRNA, in the mouse a marker for visceral endoderm that corresponds to the hypoblast in primates, by reverse transcription–PCR in day-10 colonies; data not shown), it is possible that signals from these cells or this germ layer are lacking for a proper and complete patterning. Remarkably, we observed this relatively complex embryoid body formation under culture conditions favoring the undifferentiated status above differentiation. Therefore, future experiments using stimuli for early development and embryonic patterning will help to explore the potential of the rhES cell line R366.4 in terms of its ability to develop embryonic disc–like structures and to potentially serve as a model for early developmental processes in addition to EMT.

Acknowledgments

R.B. and M.T. contributed equally to this study. We thank Prof. Dr. A. Wobus for generous support and advice. The skillful technical assistance of I. Kromberg, B. Maranca-Hüwel, D. Schünke, B. Gobs-Hevelke, and R. Brand is acknowledged with great gratitude. This study was supported in part by a grant from the Interne Forschungsförderung Essen (IFORES) to R.B. and a grant from the Kompetenznetzwerk Stammzellforschung NRW to M.T. and H.W.D.

References

1 Thomson JA, Kalishman J, Golos TG et al. Isolation of a primate embryonic stem cell line. Proc Natl Acad Sci U S A 1995;92:7844–7848.

2 Thomson JA, Kalishman J, Golos TG et al. Pluripotent cell lines derived from common marmoset (Callithrix jacchus) blastocysts. Biol Reprod 1996;55:254–259.

3 Suemori H, Tada T, Torii R et al. Establishment of embryonic stem cell lines from cynomolgus monkey blastocysts produced by IVF or ICSI. Dev Dyn 2001;222:273–279.

4 Hwang WS, Ryu YJ, Park JH et al. Evidence of a pluripotent human embryonic stem cell line derived from a cloned blastocyst. Science 2004;303:1669–1674.

5 Reubinoff BE, Pera MF, Fong CY et al. Embryonic stem cell lines from human blastocysts: somatic differentiation in vitro. Nat Biotechnol 2000;18:399–404.

6 Thomson JA, Itskovitz-Eldor J, Shapiro SS et al. Embryonic stem cell lines derived from human blastocysts. Science 1998;282:1145–1147.

7 Grabel L, Becker S, Lock L et al. Using EC and ES cell culture to study early development: recent observations on Indian hedgehog and Bmps. Int J Dev Biol 1998;42:917–925.

8 Rathjen J, Lake JA, Bettess MD et al. Formation of a primitive ectoderm like cell population, EPL cells, from ES cells in response to biologically derived factors. J Cell Sci 1999;112:601–612.

9 Rodda SJ, Kavanagh SJ, Rathjen J et al. Embryonic stem cell differentiation and the analysis of mammalian development. Int J Dev Biol 2002;46:449–458.

10 Thomson JA, Marshall VS. Primate embryonic stem cells. Curr Top Dev Biol 1998;38:133–165.

11 Schulz TC, Palmarini GM, Noggle SA et al. Directed neuronal differentiation of human embryonic stem cells. BMC Neurosci 2003;4:27.

12 Liptau H, Viebahn C. Expression patterns of gap junctional proteins connexin 32 and 43 suggest new communication compartments in the gastrulating rabbit embryo. Differentiation 1999;65:209–219.

13 Heneweer C, Adelmann HG, Kruse LH et al. Human uterine epithelial RL95-2 cells reorganize their cytoplasmic architecture with respect to Rho protein and F-actin in response to trophoblast binding. Cells Tissues Organs 2003;175:1–8.

14 Heneweer C, Kruse LH, Kindhauser F et al. Adhesiveness of human uterine epithelial RL95-2 cells to trophoblast: rho protein regulation. Mol Hum Reprod 2002;8:1014–1022.

15 Adelmann H. A frequency-domain Gaussian filter module for quantitative and reproducible high-pass, low-pass and band-pass filtering of images. Am Lab 1997;29:27–33.

16 Ciruna B, Rossant J. FGF signaling regulates mesoderm cell fate specification and morphogenetic movement at the primitive streak. Dev Cell 2001;1:37–49.

17 Damjanov I, Damjanov A, Damsky CH. Developmentally regulated expression of the cell-cell adhesion glycoprotein Cell-CAM 120/80 in peri-implantation mouse embryos and extraembryonic membranes. Dev Biol 1986;116:194–202.

18 Xu C, Inokuma MS, Denham J et al. Feeder-free growth of undifferentiated human embryonic stem cells. Nat Biotechnol 2001;19:971–974.

19 Viebahn C, Stortz C, Mitchell SA et al. Low proliferative and high migratory activity in the area of Brachyury expressing mesoderm progenitor cells in the gastrulating rabbit embryo. Development 2002;129:2355–2365.

20 Nieto MA, Sargent MG, Wilkinson DG et al. Control of cell behavior during vertebrate development by Slug, a zinc finger gene. Science 1994;264:835–839.

21 Saga Y, Hata N, Kobayashi S et al. MesP1: a novel basic helix-loop-helix protein expressed in the nascent mesodermal cells during mouse gastrulation. Development 1996;122:2769–2778.

22 Odorico JS, Kaufman DS, Thomson JA. Multilineage differentiation from human embryonic stem cell lines. STEM CELLS 2001;19:193–204.

23 Andrews PW. From teratocarcinomas to embryonic stem cells. Philos Trans R Soc Lond B Biol Sci 2002;357:405–417.

24 Damjanov I. Experimental Teratoma: Current Topics in Pathology. Berlin: Springer, 1974:69–130.

25 Denker HW. Embryonic stem cells: An exciting field for basic research and tissue engineering, but also an ethical dilemma? Cells Tissues Organs 1999;165:246–249.

26 Denker HW. Early human development: new data raise important embryological and ethical questions relevant for stem cell research. Naturwissenschaften 2004;91:1–21.

27 Dahl E, Winterhager E, Reuss B et al. Expression of the gap junction proteins connexin31 and connexin43 correlates with communication compartments in extraembryonic tissues and in the gastrulating mouse embryo, respectively. J Cell Sci 1996;109:191–197.

28 Yancey SB, Biswal S, Revel JP. Spatial and temporal patterns of distribution of the gap junction protein connexin43 during mouse gastrulation and organogenesis. Development 1992;114:203–212.

29 Reuss B, Hellmann P, Traub O et al. Expression of connexin31 and connexin43 genes in early rat embryos. Dev Genet 1997;21:82–90.

30 Peinado H, Quintanilla M, Cano A. Transforming growth factor beta-1 induces snail transcription factor in epithelial cell lines: mechanisms for epithelial mesenchymal transitions. J Biol Chem 2003;278:21113–21123.

31 Savagner P. Leaving the neighborhood: molecular mechanisms involved during epithelial-mesenchymal transition. Bioessays 2001;23:912–923.

32 Hay ED. An overview of epithelio-mesenchymal transformation. Acta Anat (Basel) 1995;154:8–20.

33 Clements D, Taylor HC, Herrmann BG et al. Distinct regulatory control of the Brachyury gene in axial and non-axial mesoderm suggests separation of mesoderm lineages early in mouse gastrulation. Mech Dev 1996;56:139–149.

34 Wilkinson DG, Bhatt S, Herrmann BG. Expression pattern of the mouse T gene and its role in mesoderm formation. Nature 1990;343:657–659.

35 Blum M, Gaunt SJ, Cho KW et al. Gastrulation in the mouse: the role of the homeobox gene goosecoid. Cell 1992;69:1097–1106.

36 Yeom YI, Fuhrmann G, Ovitt CE et al. Germline regulatory element of Oct-4 specific for the totipotent cycle of embryonal cells. Development 1996;122:881–894.

37 Ovitt CE, Scholer HR. The molecular biology of Oct-4 in the early mouse embryo. Mol Hum Reprod 1998;4:1021–1031.

38 Armstrong L, Lako M, Lincoln J et al. mTert expression correlates with telomerase activity during the differentiation of murine embryonic stem cells. Mech Dev 2000;97:109–116.

39 Nagy A, Rossant J, Nagy R et al. Derivation of completely cell culture-derived mice from early-passage embryonic stem cells. Proc Natl Acad Sci U S A 1993;90:8424–8428.